Atmospheric Environment 150 (2017) 67–76

Contents lists available at ScienceDirect

Atmospheric Environment

journal homepage: www.elsevier.com/locate/atmosenv

Secondary organic aerosol formation from photo-oxidation of toluene with NO_x and SO_2: Chamber simulation with purified air versus urban ambient air as matrix

Wei Deng [a, b], Tengyu Liu [a], Yanli Zhang [a, c, **], Shuping Situ [d], Qihou Hu [a], Quanfu He [a], Zhou Zhang [a], Sujun Lü [a, b], Xinhui Bi [a], Xuemei Wang [d], Antoinette Boreave [e], Christian George [e], Xiang Ding [a], Xinming Wang [a, c, *]

[a] State Key Laboratory of Organic Geochemistry and Guangdong Key Laboratory of Environmental Protection and Resources Utilization, Guangzhou Institute of Geochemistry, Chinese Academy of Sciences, Guangzhou 510640, China
[b] University of Chinese Academy of Sciences, Beijing 100049, China
[c] Center for Excellence in Regional Atmospheric Environment, Institute of Urban Environment, Chinese Academy of Sciences, Xiamen 361021, China
[d] School of Environmental Science and Engineering, Sun Yat-sen University, Guangzhou 510275, China
[e] Institut de Recherches sur la Catalyse et l'Environment de Lyon (IRCELYON), CNRS, UMR5256, Villeurbanne F-69626, France

HIGHLIGHTS

- Photo-oxidation of toluene/SO_2/NO_x in chamber in ambient air versus in purified air.
- Higher SOA productions and yields in matrix of ambient air than of purified air.
- Enhanced SO_2 degradation and sulfate formation in ambient air matrix.
- Higher particle acidity in ambient air matrix promoted acid-catalyzed SOA formation.
- Elevated OH levels observed in ambient air matrix than in purified air matrix.

ARTICLE INFO

Article history:
Received 11 August 2016
Received in revised form
5 November 2016
Accepted 18 November 2016
Available online 21 November 2016

Keywords:
Secondary organic aerosols
Toluene
Chamber simulation
Purified air
Ambient air
Sulfate
Particle acidity
Matrix effect

ABSTRACT

Chamber studies on the formation of secondary aerosols are mostly performed with purified air as matrix, it is of wide concern in what extent they might be different from the situations in ambient air, where a variety of gaseous and particulate components preexist. Here we compared the photo-oxidation of "toluene + NO_x + SO_2" combinations in a smog chamber in real urban ambient air matrix with that in purified air matrix. The secondary organic aerosols (SOA) mass concentrations and yields from toluene in the ambient air matrix, after subtracted ambient air background primary and secondary organic aerosols, were 9.0–34.0 and 5.6–12.9 times, respectively, greater than those in purified air matrix. Both homogeneous and heterogeneous oxidation of SO_2 were enhanced in ambient air matrix experiments with observed 2.0–7.5 times higher SO_2 degradation rates and 2.6–6.8 times faster sulfate formation than that in purified air matrix, resulting in higher in-situ particle acidity and consequently promoting acid-catalyzed SOA formation. In the ambient air experiments although averaged OH radical levels were elevated probably due to heterogeneous formation of OH on particle surface and/or ozonolysis of alkenes, non-OH oxidation pathways of SO_2 became even more dominating. Under the same organic aerosol mass concentration, the SOA yields of toluene in purified air matrix experiments matched very well with the two-product model curve by Ng et al. (2007), yet the yields in ambient air on average was over two times

* Corresponding author. State Key Laboratory of Organic Geochemistry Guangzhou Institute of Geochemistry, Chinese Academy of Sciences, China.
** Corresponding author. State Key Laboratory of Organic Geochemistry Guangzhou Institute of Geochemistry, Chinese Academy of Sciences, China.
E-mail addresses: zhang_yl86@gig.ac.cn (Y. Zhang), wangxm@gig.ac.cn (X. Wang).

http://dx.doi.org/10.1016/j.atmosenv.2016.11.047
1352-2310/

larger. The results however were much near the best fit curve by Hildebrandt et al. (2009) with the volatility basis set (VBS) approach.

1. Introduction

Fine particulate matter with a dynamic diameter less than 2.5 μm ($PM_{2.5}$) in the atmosphere affects human health, air quality, and climate (Pope et al., 2009; Parrish and Zhu, 2009; Liu et al., 2015b; Lelieveld et al., 2015). Second organic aerosols (SOA) are mainly formed from the oxidation of anthropogenic and biogenic volatile organic compounds (VOCs), and account for a substantial mass fraction of $PM_{2.5}$ in ambient air (Zhang et al., 2007). An accurate estimation of the SOA burden at the regional and global scale is therefore vital to assess the effects of organic aerosols (OA) on human health and climate.

In current regional and global chemical transport models, SOA is predicted by combining the emissions of anthropogenic or biogenic precursors and their individual SOA productivity according to data from smog chamber experiments (Hallquist et al., 2009; Barsanti et al., 2013; Mahmud and Barsanti, 2013), with a two-product model (Odum et al., 1996) and the volatility basis set (VBS) approach (Donahue et al., 2006) used as the inner core for the calculation of SOA yields. However, the modeled results are generally underestimated when compared to observed values (De Gouw et al., 2005; Volkamer et al., 2006; Hodzic et al., 2010; Hodzic and Jimenez, 2011). One reason for this discrepancy is the existence of unknown precursors, such as intermediate volatile organic compounds (IVOCs) and semi-volatile organic compounds (SVOCs) (Robinson et al., 2007; Deng et al., 2016), or unknown multiple phase processes, including aqueous chemistry (Lim et al., 2010; Ervens et al., 2014). Pye et al. (2013) and Marais et al. (2016) demonstrate that replacing a reversible partitioning approach with reactive uptake to aqueous aerosol improves agreement between models and observations. Another concern is that if the widely used SOA formation potential of VOCs based on smog chamber studies with purified air as a matrix (Surratt et al., 2007; Ng et al., 2007; Tsimpidi et al., 2010) could well represent the situations in ambient air, which is a mixture of thousands of gas and particle phase species. Kamens et al. (2011) reported that the toluene SOA formation potential was greater for the rural North Carolina background seed system than for the $(NH_4)_2SO_4$ seed, which is a widely used seed aerosol in chamber studies. Therefore, to check the matrix effect of real ambient air against purified air, more chamber studies on SOA formation need to be conducted with real air as matrix.

Aromatic hydrocarbons constitute an important fraction of nonmethane hydrocarbons (Zhang et al., 2012, 2013a), and are very important anthropogenic SOA precursors (Odum et al., 1997a, b) that account for a large portion of the SOA formation among VOCs from a variety of emission sources, such as gasoline vehicle exhaust (Nordin et al., 2013; Liu et al., 2015a). Particularly in polluted urban areas they might even dominate over biogenic volatile organic compounds in forming SOA (Ding et al., 2012; Wang et al., 2013). Toluene is among the most abundant aromatic hydrocarbons in the atmosphere (Zhao et al., 2004; Zhang et al., 2016) and as a model aromatic hydrocarbon its SOA formation potential has been extensively investigated (Edney et al., 2000; Hurley et al., 2001; Ng et al., 2007; Hildebrandt et al., 2009). These previous chamber studies, however, were all conducted in purified air. In this present study we studied SOA formation from the photo-oxidation of toluene in a smog chamber with both purified air and real urban air as matrices. The aim was to understand the difference in the SOA formation with ambient air versus purified air as matrix, and to provide useful implication for better SOA estimation in global chemical transport models.

2. Material and methods

2.1. Experiments

All experiments were performed in the smog chamber in the Guangzhou Institute of Geochemistry, Chinese Academy of Sciences (GIG-CAS). The GIG-CAS smog chamber consists of a 30 m^3 fluorinated ethylene propylene (FEP) Teflon film reactor, housed in a temperature-controlled enclosure and equipped with black lamps as the light source. Further details of the chamber setup and facilities can be found elsewhere (Wang et al., 2014). Prior to each experiment, the reactor was flushed with dry purified air for at least 48 h, which represents at least five exchanges of the reactor volume.

Temperature and relative humidity (RH) inside the chamber were set to 25 °C and 50%, respectively (Table 1). The initial concentrations of toluene and SO_2 were kept at around 80 and 100 ppbv, respectively, and NO_x levels were maintained at approximately 80 or 240 ppbv. To introduce toluene into the reactor, a fixed volume of pure liquid toluene was heated and vaporized in a heating system, with the vapor flushed into the chamber by high purity nitrogen via an injection port. After more than half an hour of mixing, the mixture inside the Teflon reactor was continuously exposed to black light for 5 h. After the black lamps were switched off, the particles that had formed were characterized for another 2–3 h to correct the wall loss.

For comparison, three groups of contrasting experiments (Expt. 1 and Expt. 5, Expt. 2 and Expt. 6, Expt. 3 and Expt. 7) were performed. In each pair of experiments, purified air and ambient air were respectively used as the matrix while the initial conditions, including temperature, RH, reactant concentrations and VOC/NO_x ratios, were kept similar between the two experiments (Table 1). In the experiments with ambient air as the matrix, the Teflon reactor was vented and refilled at least twice with real urban outdoor air from Guangzhou, China, using a pump with a flow rate of 1.13 m^3 min^{-1}. No seed particles were introduced for the experiments with purified air except that in Expt. 4, initial conditions were identical to that in Expt.1 with purified air as the matrix but we injected ammonium sulfate seed particles with a final number concentration of about 6500 cm^{-3}. By comparing results of Expt.4 with that of Expt.1, we can evaluate the impact of seed particles and vapor wall loss.

The total concentration of background VOCs was negligible compared with the high concentration of toluene (Table S1). However, Robinson et al. (2007) reported that SVOCs and IVOCs were potentially a large source of SOA. To obtain accurate concentrations of the SOA produced by toluene (*Tol*-SOA) in ambient air experiments, a blank experiment (Expt. bk) was designed to estimate the SOA formation from both gas and particle phase species in the ambient air. In Expt. bk, all of the operating procedures and conditions were similar to those ambient air matrix experiments,

Table 1
Initial conditions and final results for chamber experiments.

Expt.No.	Matrix	Seed[a]	T (°C)	RH (%)	OH (× 10^6 molecules cm^{-3})	NO (ppbv)	NO_2 (ppbv)	SO_2 (ppbv)	Toluene (ppbv)	ΔToluene (ppbv)	O_3[b] (ppbv)	ΔM_0[c] (μg m^{-3})	SOA yield[d]
1	Purified air	none	25.8	52.8	2.83	69.7	2.5	104.4	79.6	23.0	77.6	7.0	8.2%
2	Purified air	none	25.9	50.7	1.78	222.4	10.2	98.7	62.1	14.7	7.6	2.1	3.8%
3	Purified air	none	25.4	50.5	1.56	10.7	78.3	125.9	75.5	10.8	42.7	0.8	2.0%
4	Purified air	AS	26.9	55.5	2.94	62.0	6.2	95.2	73.4	20.7	68.3	6.2	8.0%
5	Ambient air	BGS	24.6	51.4	3.40	62.4	24.3	132.6	84.5	37.0	58.1	78.1	46.1%
6	Ambient air	BGS	25.0	52.8	4.54	177.5	50.8	108.6	85.3	31.9	21.9	39.3	31.4%
7	Ambient air	BGS	25.3	51.4	3.73	0.3	76.9	106.1	89.9	28.0	73.0	29.1	25.7%
bk	Ambient air	BGS	26.0	63.7	–	21.6	42.4	100.3	–	–	83.5	10.7	–

[a] AS is ammonium sulfate, BGS represents background ambient air seeds.
[b] The maximum concentration of ozone during experiments.
[c] Wall-loss corrected SOA mass concentration measured by HR-ToF-AMS.
[d] Assuming an SOA density of 1.4 g cm^{-3}.

except that no toluene was added (Table 1). 10.7 μg m^{-3} of SOA was formed in blank experiment. The method used to estimate *Tol*-SOA is described in the Supporting Information (SI).

2.2. Instrumentation

A series of instruments were used to characterize the gas and particle phase compounds in the reactor. Gas-phase ozone (O_3) and NO_x were measured online with dedicated monitors (EC9810 and 9841T; Ecotech, Knoxfield, Australia). Sulfur dioxide was measured with a Thermo Scientific Model 43i analyzer. Gas phase organic species were measured with an automated preconcentrator (Model 7100; Entech Instruments Inc., Simi Valley, CA, USA), coupled with a gas chromatography-mass selective detector/flame ionization detector/electron capture detector (GC-MSD/FID/ECD) (Model 5973N; Agilent Technologies, Santa Clara, CA, USA) (Wang and Wu, 2008; Zhang et al., 2010, 2013b) and a commercial proton-transfer-reaction time-of-flight mass spectrometer (PTR-ToF-MS) (Model, 2000; Ionicon Analytik GmbH, Innsbruck, Austria) (Lindinger et al., 1998; Jordan et al., 2009). The average OH concentration for each experiment was estimated by the decay of toluene (Liu et al., 2016), which was measured online by the PTR-ToF-MS. Calculated OH concentrations ranged 1–4 × 10^6 molecules cm^{-3} in the experiments (Table 1).

Particle number concentrations and size distributions were measured with a scanning mobility particle sizer (SMPS) (Model 3080 classifier) and condensation particle counter (CPC) (Model 3775; both from TSI Inc., Shoreview, MN, USA). An aerosol density of 1.4 g cm^{-3} was assumed to convert the particle volume concentration into the mass concentration (Ng et al., 2007). A high-resolution time-of-flight aerosol mass spectrometer (HR-ToF-AMS) (Aerodyne Research Inc., Billerica, MA, USA) was used to measure the chemical composition of particles and the non-refractory submicron aerosol mass (Jayne et al., 2000; DeCarlo et al., 2006). The toolkit Squirrel 1.51H was used to obtain the time series of various mass components (sulfate, nitrate, ammonium, and organics). The contribution of gas-phase CO_2 to the *m/z* 44 signal was corrected with measured CO_2 concentrations. In addition, AMS tend to underestimate the PM mass due to poor transmission for particles with diameter smaller than 70 nm (aerodynamic diameter) (Jayne et al., 2000). Fig. S1 plotted the particle volume concentration measured by SMPS for Expt. 1. Particles with diameter smaller than 50 nm (mobility diameter) accounted for less than 10% of total particle mass, indicating HR-ToF-MS might underestimate the PM in the early stage of SOA formation. To eliminate this effect, the aerosol mass measured by the AMS was corrected with SMPS data using the same method as Gordon et al. (2014) and Liu et al. (2015a). The HR-ToF-AMS was calibrated using 300 nm monodisperse ammonium nitrate particles.

2.3. Wall loss correction

The loss of particles and condensable organic vapors onto the reactor walls need to be corrected to accurately quantify total SOA production. We used the same method as Weitkamp et al. (2007) to correct the wall loss of the particles. Briefly, the change in the suspended particle mass in the chamber C_{OA}^{sus} is given by:

$$\frac{d}{dt}\left[C_{OA}^{sus}\right] = -k \cdot C_{OA}^{sus} + P_{sus} \quad (1)$$

where k represents the wall loss rate constant of aerosol mass and was determined by fitting the SMPS and AMS data after switched off the UV lamps. $k \cdot C_{OA}^{sus}$ is the loss rate of organic particle to the chamber walls, P_{sus} is the production rate of suspended SOA. The change in organic particle on the chamber walls C_{OA}^{wall} is:

$$\frac{d}{dt}\left[C_{OA}^{wall}\right] = k \cdot C_{OA}^{wall} + P_{wall} \quad (2)$$

where P_{wall} is the net rate of mass transfer of organics to the chamber walls. To determine P_{wall}, we assume that the rate of organic vapors uptake to particles on the wall is related to the ratio of total particle mass on the walls to that in suspension (Weitkamp et al., 2007):

$$P_{wall} = P_{sus}\left(\frac{\omega C_{wall}}{C_{sus}}\right) \quad (3)$$

where C_{wall} is the total particle mass deposited on the chamber walls, C_{sus} is the measured total particle mass concentrations, and ω is a proportionality factor of organic vapor partitioning to chamber walls and suspended particles (Weitkamp et al., 2007). P_{sus} can be determined by Equation (1). Then we can integrate Equation (2) to determine C_{OA}^{wall} and obtain the total concentration of organic aerosol according to: $C_{OA} = C_{OA}^{sus} + C_{OA}^{wall}$. Two limiting cases were considered: $\omega = 0$ when no organic vapors condense to wall-bound particles; and $\omega = 1$ when organic vapors remain in equilibrium with both wall-bound and suspended particles.

Besides uptake to the wall-bound particles, organic vapors can also be lost to the chamber walls via deposition on the chamber wall directly, and thus significantly impact SOA formation (Yeh and Ziemann, 2014; Zhang et al., 2014, 2015; Ye et al., 2016b). To examine the influence of vapor wall loss, in Expt. 4 ammonium sulfate was injected into the chamber as seed particles. We found that both the SOA mass and yield are comparable with that in Expt. 1, in which no seed aerosols were introduced. As discussed in Section 3.2, the difference of SOA formation between purified and ambient air experiments is not caused by the vapor wall loss to the Teflon chamber, neglecting the direct deposition of organic vapors

to the chamber wall will not bias our conclusions. In this study, to facilitate the comparison of our results with that in previous studies (Ng et al., 2007; Hildebrandt et al., 2009), we neglected the direct deposition of organic vapors to the chamber wall just as did in the previous studies. Therefore, the total organic mass concentration calculated in this study is only the lower bound, which could underestimate the SOA formation.

2.4. Characterization of ambient air

The compositions of main background VOCs in experiments with ambient air are shown in Table S1. Except for short-chain alkanes, the total concentration of background VOCs was negligible compared with the high concentration of toluene while these short-chain alkanes are not SOA precursors. In three ambient air matrix experiments, the initial mass concentrations of background seed aerosols were 9.3, 8.1, and 12.7 μg m^{-3}, and the particle number concentrations were 6,234, 8,013, and 14,649 cm^{-3}, respectively (Table S2). The particle number distributions for these three experiments are shown in Fig. S2. Particles less than 200 nm dominated in particle number concentrations, consistent with ambient air observations in the Pearl River Delta (Liu et al., 2008; Yue et al., 2010). The chemical compositions of the initial aerosols in ambient air experiments were characterized by HR-ToF-AMS and were presented in Table S2. OA dominated the non-refractory aerosol mass (47.3% for Expt. 5, 45.7% for Expt. 6, and 59.1% for Expt. 7), followed by sulfate (35.5% for Expt. 5, 22.2% for Expt. 6, and 11.8% for Expt. 7), nitrate (5.4% for Expt. 5, 19.8% for Expt. 6, and 20.5% for Expt. 7) and ammonium (11.8% for Expt. 5, 12.3% for Expt. 6, and 8.7% for Expt. 7), which were quite similar to ambient aerosol results reported in Guangzhou in previous studies (Wang et al., 2012; Fu et al., 2014; Huang et al., 2014).

3. Results and discussion

3.1. SOA formation

Fig. 1 presents aerosol mass concentration as a function of toluene consumption for three pure air experiments. A delay of SOA formation from initial consumption of toluene is observed, suggesting that SOA is mainly formed by further oxidation of first-generation products (Bowman et al., 1997; Hurley et al., 2001). SOA formation from aromatic hydrocarbons photo-oxidation is reported to be highly sensitive to NO concentration (Li et al., 2015). For NO initiated experiments (Expt. 1 and Expt. 2), we noticed that the experiment with higher VOC/NO_x ratio produced more organic aerosol than the lower VOC/NO_x ratio experiment at the same toluene consumption, which is consistent with previous studies (Song et al., 2005; Ng et al., 2007). However, the NO_2 initiated experiment (Expt. 3) demonstrated different SOA growth (Fig. 1), with the formed SOA mass lower than that for NO initiated experiments when the same amount of toluene was consumed. Nishino et al. (2010) revealed that the yields of glyoxal and methylglyoxal from reactions of toluene decreased with increasing NO_2 concentration. As glyoxal and methylglyoxal are regarded as very important SOA precursors through uptake into water or/and heterogeneous reaction, their different yields at NO and NO_2 initiated conditions would further induce the different SOA growth (Lim et al., 2010; Kamens et al., 2011).

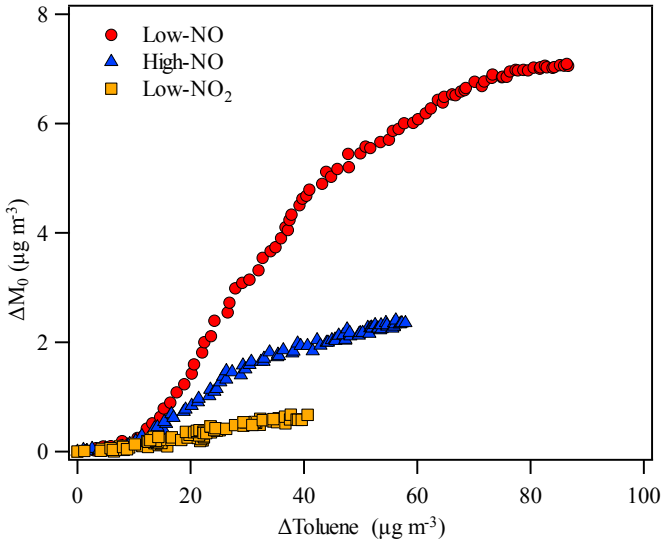

Fig. 1. Time dependent growth curves for purified air experiments. Low-NO represents Expt. 1, high-NO represents Expt. 2 and low-NO_2 represents Expt. 3.

Fig. 2 shows a comparison of the *Tol*-SOA time series for experiments with ambient air matrix against that with purified air matrix during 5 h of irradiation. The plotted *Tol*-SOA data are the values after wall loss correction and with background OA deducted. The *Tol*-SOA mass in ambient air matrix experiments was estimated using the high resolution AMS data. After 5 h of photo-oxidation, the concentrations of *Tol*-SOA in ambient air matrix experiments were 64.4 (Expt.5), 37.7 (Expt.6) and 27.1 μg m^{-3} (Expt. 7), respectively, approximately 9–34 times that in the parallel purified air matrix experiments (7.0 μg m^{-3} for Expt. 1, 2.1 μg m^{-3} for Expt. 2, and 0.8 μg m^{-3} for Expt. 3). The average *Tol*-SOA growth rate within 2 h after SOA was climbing in Expt. 5 with ambient air as matrix was calculated to be 14.8 μg m^{-3} h^{-1}, over one order of magnitude higher than that of 1.1 μg m^{-3} h^{-1} in Expt. 1 with purified air as matrix. However, as shown in Table 1, the amounts of toluene consumed in the three ambient air matrix experiments (37.0, 31.9, and 28.0 ppbv, respectively) were only less than three times that reacted in the purified air matrix experiments (23.0, 14.7, and 10.8 ppbv, respectively). Thus, the huge discrepancy in the *Tol*-SOA mass formed or *Tol*-SOA growth rate between the purified air and ambient air experiments cannot be solely explained by the amounts of toluene oxidized.

The SOA yield *Y* has been used to represent the organic aerosol formation potential in models (Grosjean and Seinfeld, 1989; Odum et al., 1996, 1997a). The toluene SOA yield *Y*, defined as the fraction of consumed toluene that is converted to aerosols by means of atmospheric oxidation, is calculated by:

$$Y = \frac{\Delta M_0}{\Delta Tol} \quad (4)$$

where ΔM_0 is the SOA mass concentration (μg m^{-3}) formed by toluene and ΔTol represents the amount of toluene reacted (μg m^{-3}) during the photo-oxidation. As shown in Table 1, the SOA yields of the three ambient air matrix experiments were 46.1%, 31.4%, and 25.7%, respectively, which were 5.6–12.9 times that of the parallel purified air matrix experiments.

3.2. The effect of seed particles

Recent studies have indicated that the existence of high concentrations of seed particles might promote gas-particle partition and decrease the loss of organic vapors to the walls, thus enhance SOA formation (Zhang et al., 2014, 2015; Ye et al., 2016b). In this study, we injected ammonium sulfate as seed particles in Expt. 4 with a number concentration of ~6500 cm^{-3}. The particle number distribution was presented in Fig. S2. The seed particles had a

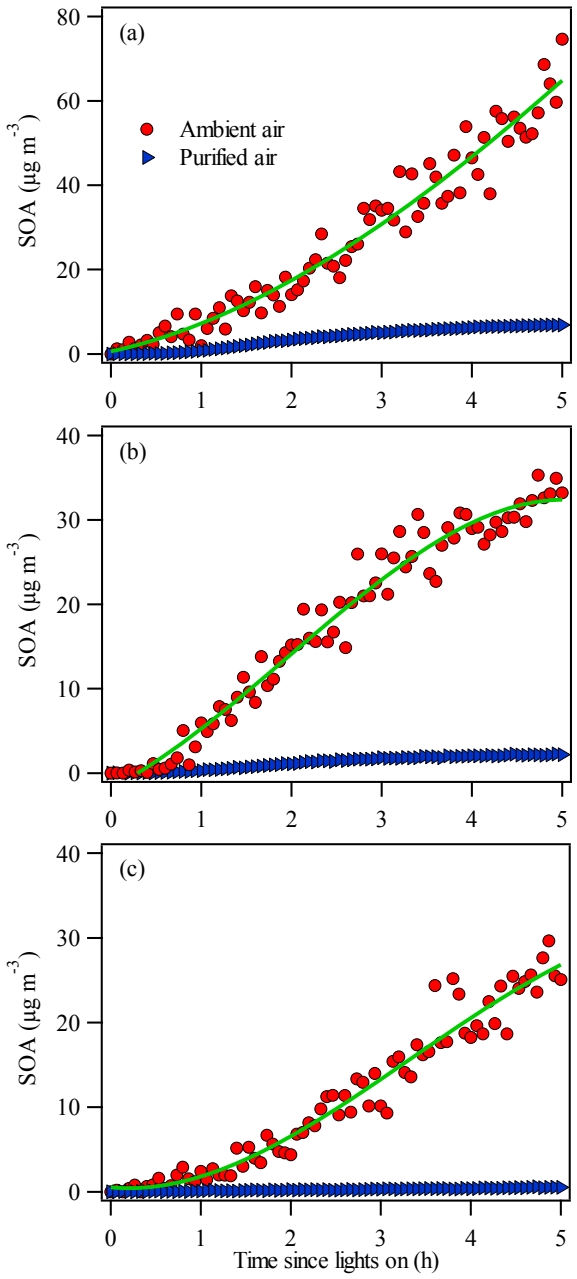

Fig. 2. Concentration of wall-loss corrected *Tol*-SOA derived from AMS data in ambient air experiment (red) and purified air experiment (blue) during 5 h of irradiation. (a) low NO condition (80 ppbv NO, Expt. 1 and 5), (b) high NO condition (200 ppbv NO, Expt. 2 and 6), (c) low NO_2 (80 ppbv NO_2, Expt. 3 and 7). Green lines are the best fits of the data. (For interpretation of the references to colour in this figure legend, the reader is referred to the web version of this article.)

surface area (SA) of 470 μm^2 cm^{-3}, which was similar to or even higher than that in the ambient air matrix experiments (181–456 μm^2 cm^{-3}). However, the SOA yield (8.0%) in Expt. 4 was comparable to that observed in the experiment without any seed aerosols (8.2%, Expt. 1), and less than 20% of that in Expt. 5 (46.1%; ambient air matrix). In the three parallel experiments (Expt. 1, 4 and 5), after the lights were turned on for about 30 min, particle number concentrations all increased significantly to over 1,000,000 cm^{-3} with new particle formation (Fig. 3). Additionally, as showed in Fig. 4, the particle SA in Expt. 1 (purified air matrix) increased to over 100 μm^2 cm^{-3} in 20 min and became almost the same of that in Expt. 5 (ambient air matrix). Hence, the above facts suggested that the loss of organic vapors directly onto the walls is not the reason for the discrepancy of SOA formation between ambient air experiments and purified air experiments and that seed aerosols could not explain the substantially elevated SOA yields in the ambient air matrix experiments. This is consistent with a previous study, which reported that no measured differences were observed in SOA formation from m-xylene between the non-seeded and seeded experiments (Li et al., 2015).

Aerosols in ambient air, however, are not just inorganics like ammonium sulfate; they also contain a substantial fraction of organics. Previous studies revealed that preexisting particle-bound organics can enhance SOA formation through suppressing the evaporation of SOA and shifting the partitioning equilibrium to the particle phase (Odum et al., 1996; Kamens et al., 2011; Ye et al., 2016a). As determined by AMS, approximate half of the particle mass in the matrix ambient air was comprised of organic matters for Expt. 5–7 (Table S2). This might partly explain the enhanced SOA formation with ambient air as the matrix. However, in the experiments bathing with ambient air, as determined by AMS the initial OA concentrations were 4.4, 3.7 and 7.5 μg m^{-3} (Table S2), respectively. With the SOA yield curves depicted in Fig. 5, for either the two-product model or the VBS approach, an incremental of M_0 less than 8.0 μg m^{-3} would not induce the increase of SOA yields as high as observed in the ambient air matrix experiments in the present study. Therefore, the enhancement of SOA yields in ambient air matrix could not be largely explained by the existing background OA.

3.3. The effect of particle acidity

Particle acidity can significantly facilitate SOA formation from toluene (Cao and Jang, 2007). The in-situ particle acidity just before the lights were turned on and when SOA formation rates peaked, were calculated as H^+ concentrations based on the AIM-II model for the H^+–NH_4^+–SO_4^{2-}–NO_3^-–H_2O system (Table S2) (http://www.aim.env.uea.ac.uk/aim/model2/model2a.php) (Clegg et al., 1998; Wexler and Clegg, 2002; Fu et al., 2015; Liu et al., 2016). When the SOA formation rates peaked, the in-situ particle acidities for ambient air matrix experiments were 2.35–3.81 nmol m^{-3}, about 12–64 times of that for purified air matrix experiments (Fig. 6), suggesting higher particle acidity could be the reason for the enhanced toluene SOA formation in the ambient air matrix experiments. Ng et al. (2007) observed SOA yields from aromatics in the presence of acidic seed were comparable with those using neutral seed aerosol, possibly because the relative humidity they used was approximate 5% and the aerosol water content was low. Aerosol water is essential for acidity effect (Jang et al., 2006; Cao and Jang, 2007). Liquid water content (LWC) for initial seed particles was also estimated by the AIM-II model and presented in Table S2. The aerosol water for background particles in ambient air experiments ranged from 0.43 to 0.82 μg m^{-3}, averaged 1/3 of that in $(NH_4)_2SO_4$ seeded experiment (Expt. 4), demonstrating aerosol water content is not the main factor for SOA enhancement. Kamens et al. (2011) found that the SOA mass for experiments with background seed were higher than those for $(NH_4)_2SO_4$ seeded experiments even with similar LWC in seed aerosols. Besides, Xu et al. (2015) revealed that particle water did not influence isoprene OA formation. Therefore, aerosol water might be an essential factor for acidity effect, but it is not a limiting parameter for toluene SOA formation in this study. As the particle acidity for ambient air in Guangzhou is 13 ± 4 nmol m^{-3} (Fu et al., 2015), much higher than that for chamber experiments in this study. The SOA yields in real atmospheric condition might be even higher. Thus the particle acidity effect should be considered in future model work.

It is worth noting that the initial particle acidities for ambient air

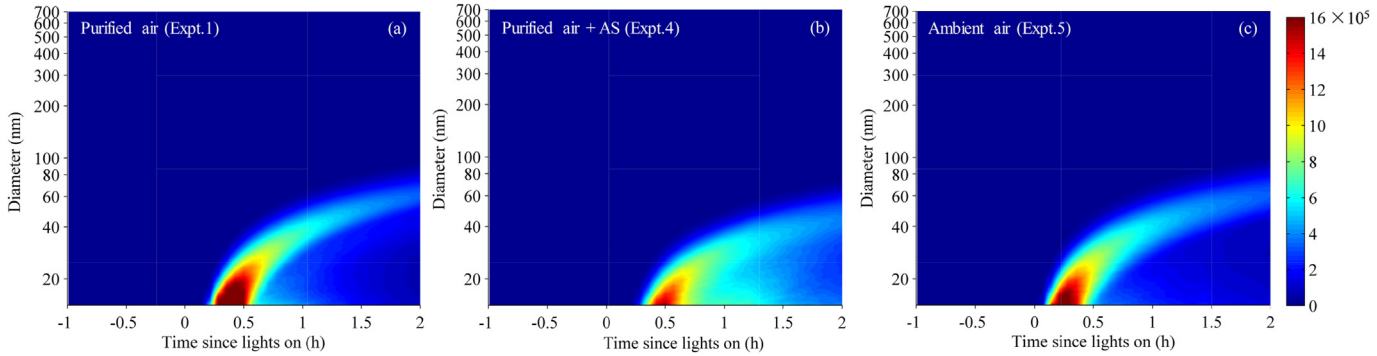

Fig. 3. Particle size-number distributions for (a) purified air experiment without $(NH_4)_2SO_4$ (Exp.1), (b) purified air experiment with $(NH_4)_2SO_4$ (Exp.4) and (c) ambient air experiment (Exp.5).

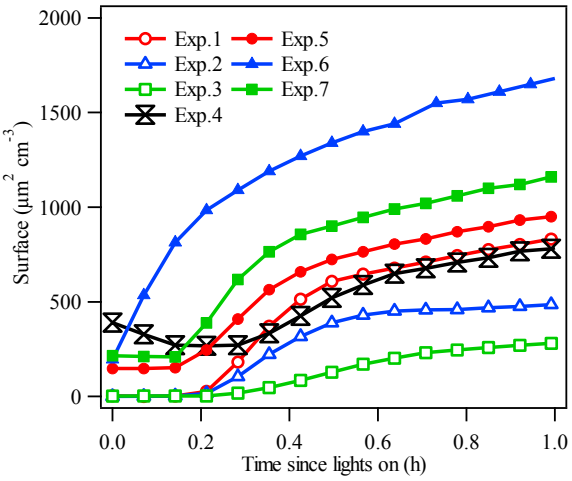

Fig. 4. Evolutions of surface areas for all experiments measured by SMPS in 1 h after lights were turned on. Line with open symbols represent purified air experiments, line with solid symbols represent ambient air experiments. Circle represents low NO condition (80 ppbv NO), triangle represents high NO condition (200 ppbv NO), square represents low NO_2 condition (80 ppbv NO_2).

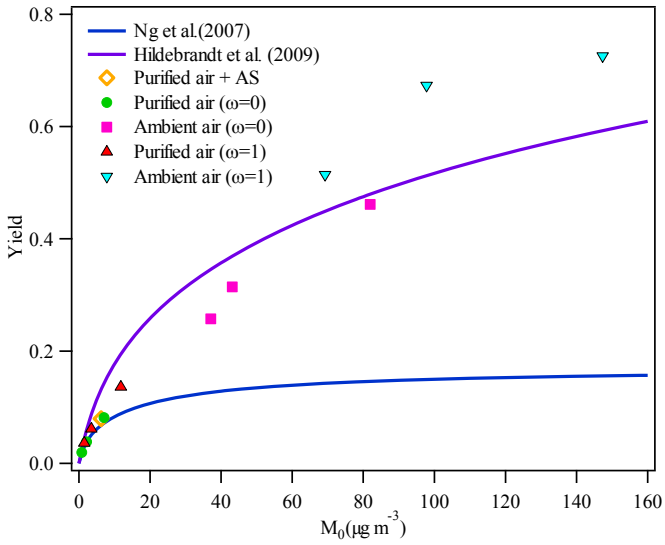

Fig. 5. Comparison of yield data obtained from toluene experiments in this study with those of Ng et al. (2007) and Hildebrandt et al. (2009), the organic aerosol density was assumed to be $\rho = 1.4$ g cm^{-3}. The light blue line is the best fit two-product model ($\alpha_1 = 0.065$, $K_{om,1} = 0.381$; $\alpha_2 = 0.128$, $K_{om,2} = 0.042$) for the data set of Ng et al. (2007). The purple line is the best fit VBS model for the data set of Hildebrandt et al. (2009) at 20 °C for high NO_x condition. (For interpretation of the references to colour in this figure legend, the reader is referred to the web version of this article.)

matrix experiments were similar to the experiment with purified air plus $(NH_4)_2SO_4$ seeds (Table S2). This means that the difference in particle acidity hereafter was caused by secondarily formed sulfate. As shown in Fig. 7, the concentrations of newly formed sulfate after 5 h of irradiation in three ambient air matrix experiments increased to 41.3, 30.5, and 27.0 μg m^{-3}, respectively, which were 2.6–6.8 times that of 15.8, 7.6, and 4.0 μg m^{-3}, respectively, in the three purified air matrix experiments. Meanwhile, the degradation rates of SO_2 for ambient air matrix experiments were approximately 2.0–7.5 times that for purified air matrix experiments. Thus, the enhancement of sulfate could be caused by the increase in SO_2 oxidation rate. Sulfate is generally deemed to be formed by the oxidation of SO_2 by OH radicals (Calvert et al., 1978), or by H_2O_2 and O_3 through in-cloud processes in the aqueous phase (Lelieveld and Heintzenberg, 1992). The initial SO_2 mixing ratios were kept almost the same during the experiments, while calculated OH concentrations in ambient air matrix experiments were 1.2–2.6 times that in pure air matrix experiments (Table 1). As no additional OH precursor (H_2O_2 or HONO) was added in this work, the enhancement of OH in ambient air could possibly be the result of heterogeneous formation of OH. It has been reported that mineral dust surfaces may act as a source of OH under UV radiation (Dupart et al., 2012), and HONO can be formed through heterogeneous photochemistry in the presence of ambient particles and NO_x (Alvarez et al., 2012; Gligorovski et al., 2015). In addition, alkenes in ambient air reached approximate 4 ppbv, which were proved to be an important source of OH radicals by reacting with ozone (Alam et al., 2013).

As presented in Fig. 8, the SO_2 loss rates through homogeneous reaction with OH radical in three purified air experiments ranged from 0.011 to 0.020 h^{-1}, accounting for 40–65% of total SO_2 degradation; in ambient air matrix experiments SO_2 loss rates through homogeneous reaction with OH radical increased to 0.024–0.033 h^{-1}, but instead only explained 21–38% of total SO_2 degradation. This indicates that there might be other processes leading to the oxidation of SO_2. Liu et al. (2016) reported that oxidation by stabilized Criegee intermediates (sCIs) formed from alkenes reacting with ozone could dominate the conversion of SO_2. Based on the concentrations of ozone and alkenes, the oxidation rates of SO_2 due to the reactions with sCIs was estimate to be $0.8–5.7 \times 10^{-5}$ h^{-1} by the method of Liu et al. (2016), accounting for less than 0.1% of total SO_2 consumption. Heterogeneous reactions the surface of mineral dusts also can accelerate the conversion of SO_2 to H_2SO_4 (Dupart et al., 2012; Yang et al., 2016). Since

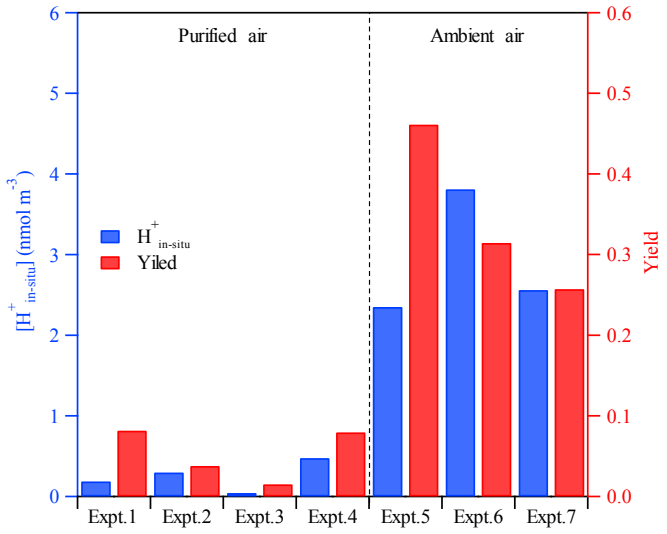

Fig. 6. In-situ particle acidities and SOA yields for all experiments. The concentration of H^+ in particle phase shown here was the value when the SOA formation rate reached the maximum during each experiment.

particles were removed in the purified air, whereas the ambient air contained heavy metals in the particulate phase (Hu et al., 2012), therefore SO_2 oxidation other than the gas-phase OH pathway became much more dominated in the ambient air matrix experiments, particularly in the early photo-oxidation.

3.4. Comparison to previous studies

Fig. 5 shows a comparison of SOA yield data obtained from this study with that reported in previous studies (Ng et al., 2007; Hildebrandt et al., 2009). The *Tol*-SOA yield curve by Ng et al. (2007) is based on the two-product model with purified air matrix chamber studies under high-NO_x conditions, and the yield parameters are widely used in chemical transport models to predict the SOA budget. The yield curve of Hildebrandt et al. (2009) is the best fit of chamber results under a high NO_x situation using the VBS approach. The experimental conditions in this study were quite different from previous studies, such as the introduction of SO_2 and absence of OH precursors (HONO or H_2O_2) in this study. However, the averaged OH concentrations were at the same level for comparison. The SOA yields of the three purified air matrix experiments fit quite well with the yield curve of Ng et al. (2007). The SOA yields from our purified air matrix experiments were 8.2%, 3.8%, and 2.0%, quite near that of 6.8%, 3.9%, and 2.4% based on the yield curve of Ng et al. (2007) under same M_0 concentrations, respectively. However, under the same M_0 concentrations the SOA yields in our ambient air matrix experiments were 2.0–3.2 times of those based on the yield curve of Ng et al. (2007). The yields obtained in this study were lower than that reported in Hildebrandt et al. (2009). The possible reason could be the yields in this research were not corrected for the loss of organic vapors to the wall particles. After considering the loss of vapors to the wall-bound particles, the yields in ambient air experiments were 72.6, 67.3 and 51.4% respectively, 1.1–1.3 times above the yield curve of Hildebrandt et al. (2009) under same M_0, while the yields in pure air matrix were approximate 70.1–81.7% of that under same M_0. Therefore, the yields in ambient air experiments could have also been underestimated according to the SOA yield curve by Hildebrandt et al. (2009), but to a much less extent.

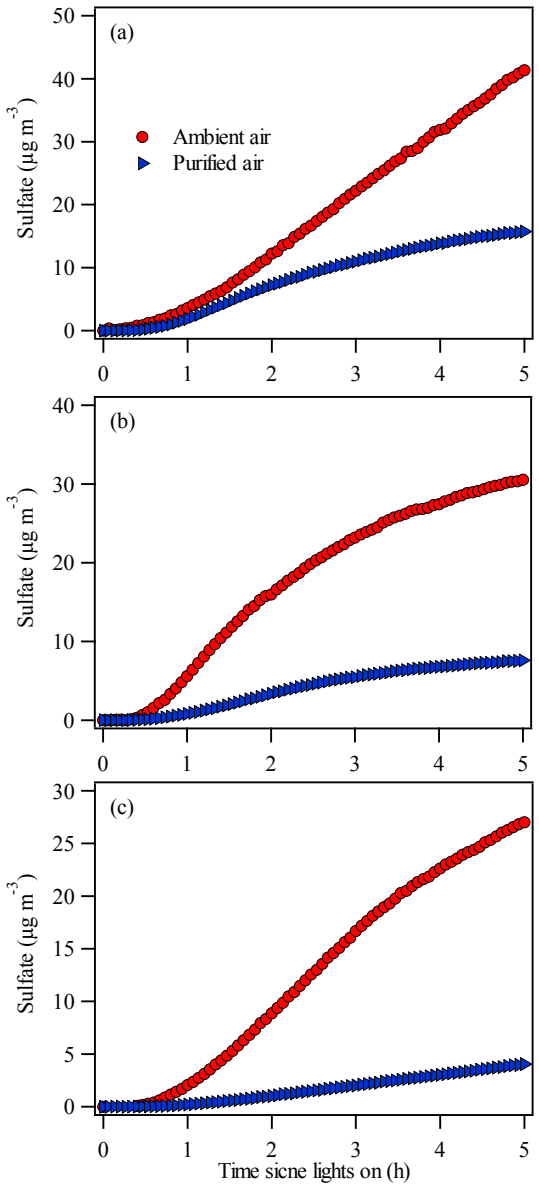

Fig. 7. Concentration of wall loss corrected sulfate derived from AMS data in ambient air experiment (red) and purified air experiment (blue) during 5 h of irradiation. (a) low NO condition (80 ppbv NO, Expt. 1 and 5), (b) high NO condition (200 ppbv NO, Expt. 2 and 6), (c) low NO_2 (80 ppbv NO_2, Expt. 3 and 7). (For interpretation of the references to colour in this figure legend, the reader is referred to the web version of this article.)

4. Conclusions

In this study, SOA formation from the photo-oxidation of toluene with NO_x and SO_2 were investigated in a smog chamber with real urban ambient air as matrix against that with purified air as matrix. We found that the *Tol*-SOA yields reached 26–46% in the ambient air matrix experiments, and they were 5.6–12.9 times higher than that in the parallel purified air matrix experiments. In ambient air matrix experiments, the averaged OH concentrations were 1.2–2.6 times that in pure air matrix experiments, probably due to heterogeneous formation of OH on particle surface and/or by ozonolysis of alkenes. These elevated OH concentrations can lead to faster oxidation rate of toluene and thus promote SOA formation (Ng et al., 2007) on the one hand; it also can accelerate the

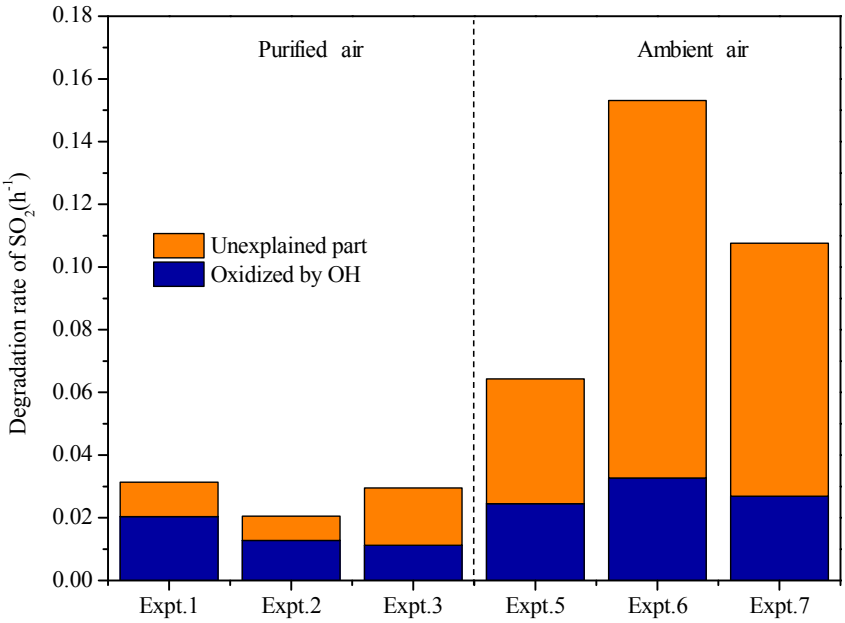

Fig. 8. The degradation rate of SO_2 during purified and ambient air experiments. The oxidation rate of SO_2 reacting with OH was calculated by the reaction rate coefficient and the average OH concentration.

oxidation of SO_2 on the other. In ambient air matrix experiments, except for enhanced oxidization by OH radical, SO_2 oxidation through other processes, such as heterogeneous reactions on the particle surface, became even more dominating. The SO_2 degradation rates in ambient air matrix were 2.0–7.5 times of that in purified air with 2.6–6.8 times faster formation rate of sulfate. The enhancement of sulfate formation resulted in much higher in-situ particle acidity, which raised both the Tol-SOA productions and yields in ambient air matrix experiments. We observed that toluene SOA yields in ambient air matrix were larger than that in previous studies (Ng et al., 2007; Hildebrandt et al., 2009) performed in purified air matrix. The present study reveals the importance of heterogeneous processes and acid-catalyzed SOA formation in the formation of secondary aerosols in real ambient air, and incorporating these processes into the models would benefit more accurate estimation of secondary aerosols. In this study, both the gas and particle phase compositions for background air were quite variable, which could lead to large uncertainties for SOA yields. Further studies are needed to elucidate the mechanism behind the difference, to parameterize the situation in ambient air, and to make clear factors impacting SOA formation in real atmospheric condition.

Supporting information

Further details of concentrations of background VOCs and particle number distributions of initial seeds in experiments with ambient air. The method of quantifying *Tol*-SOA.

Acknowledgments

This study was supported by Strategic Priority Research Program of the Chinese Academy of Sciences (Grant No. XDB05010200/KJZD-EW-TZ-G06-03), and National Natural Science Foundation of China (Grant No. 41530641/41571130031).

Appendix A. Supplementary data

Supplementary data related to this article can be found at http://dx.doi.org/10.1016/j.atmosenv.2016.11.047.

References

Alam, M.S., Rickard, A.R., Camredon, M., Wyche, K.P., Carr, T., Hornsby, K.E., Monks, P.S., Bloss, W.J., 2013. Radical product yields from the ozonolysis of short chain alkenes under atmospheric boundary layer conditions. J. Phys. Chem. A 117, 12468–12483. http://dx.doi.org/10.1021/jp408745h.

Alvarez, G.E., Wortham, H., Strekowski, R., Zetzsch, C., Gligorovski, S., 2012. Atmospheric photosensitized heterogeneous and multiphase reactions: from outdoors to indoors. Environ. Sci. Technol. 46, 1955–1963. http://dx.doi.org/10.1021/es2019675.

Barsanti, K.C., Carlton, A.G., Chung, S.H., 2013. Analyzing experimental data and model parameters: implications for predictions of SOA using chemical transport models. Atmos. Chem. Phys. 13, 12073–12088. http://dx.doi.org/10.5194/acp-13-12073-2013.

Bowman, F.M., Odum, J.R., Seinfeld, J.H., Pandis, S.N., 1997. Mathematical model for gas-particle partitioning of secondary organic aerosols. Atmos. Environ. 31, 3921–3931. http://dx.doi.org/10.1016/S1352-2310(97)00245-8.

Calvert, J.G., Su, F., Bottenheim, J.W., Strausz, O.P., 1978. Mechanism of the homogeneous oxidation of sulfur dioxide in the troposphere. Atmos. Environ. 1967 (12), 197–226. http://dx.doi.org/10.1016/0004-6981(78)90201-9.

Cao, G., Jang, M., 2007. Effects of particle acidity and UV light on secondary organic aerosol formation from oxidation of aromatics in the absence of NO_x. Atmos. Environ. 41, 7603–7613. http://dx.doi.org/10.1016/j.atmosenv.2007.05.034, 2007.

Clegg, S.L., Brimblecombe, P., Wexler, A.S., 1998. Thermodynamic model of the system H^+–NH_4^+–SO_4^{2-}–NO^{3-}–H_2O at tropospheric temperatures. J. Phys. Chem. A 102, 2137–2154. http://dx.doi.org/10.1021/jp973042r.

De Gouw, J.A., Middlebrook, A.M., Warneke, C., Goldan, P.D., Kuster, W.C., Roberts, J.M., Fehsenfeld, F.C., Worsnop, D.R., Canagaratna, M.R., Pszenny, A.A.P., Keene, W.C., Marchewka, M., Bertman, S.B., Bates, T.S., 2005. Budget of organic carbon in a polluted atmosphere: results from the New England air quality study in 2002. J. Geophys. Res. 110, D16305. http://dx.doi.org/10.1029/2004JD005623.

DeCarlo, P.F., Kimmel, J.R., Trimborn, A., Northway, M.J., Jayne, J.T., Aiken, A.C., Gonin, M., Fuhrer, K., Horvath, T., Docherty, K.S., Worsnop, D.R., Jimenez, J.L., 2006. Field-deployable, high-resolution, time-of-flight aerosol mass spectrometer. Anal. Chem. 78, 8281–8289. http://dx.doi.org/10.1021/ac061249n.

Deng, W., Hu, Q., Liu, T., Wang, X., Zhang, Y., Ding, X., Sun, Y., Bi, X., Yu, J., Yang, W., Huang, X., Zhang, Z., Huang, Z., He, Q., Mellouki, A., George, C., 2016. Chamber simulation on the formation of secondary organic aerosols (SOA) from diesel vehicle exhaust in China. Atmos. Chem. Phys. Discuss. 2016, 1–46. http://dx.doi.

org/10.5194/acp-2016-50.
Ding, X., Wang, X.M., Gao, B., Fu, X.X., He, Q.F., Zhao, X.Y., Yu, J.Z., Zheng, M., 2012. Tracer-based estimation of secondary organic carbon in the Pearl River Delta, South China. J. Geophys. Res. 117, 1–14. http://dx.doi.org/10.1029/2011JD016596.
Donahue, N.M., Robinson, A.L., Stanier, C.O., Pandis, S.N., 2006. Coupled partitioning, dilution, and chemical aging of semivolatile organics. Environ. Sci. Technol. 40, 2635–2643. http://dx.doi.org/10.1021/es052297c.
Dupart, Y., King, S.M., Nekat, B., Nowak, A., Wiedensohler, A., Herrmann, H., David, G., Thomas, B., Miffre, A., Rairoux, P., D'Anna, B., George, C., 2012. Mineral dust photochemistry induces nucleation events in the presence of SO_2. Proc. Natl. Acad. Sci. U. S. A. 109, 20842–20847. http://dx.doi.org/10.1073/pnas.1212297109.
Edney, E.O., Driscoll, D.J., Speer, R.E., Weathers, W.S., Kleindienst, T.E., Li, W., Smith, D.F., 2000. Impact of aerosol liquid water on secondary organic aerosol yields of irradiated toluene/propylene/NO_x/$(NH_4)_2SO_4$/air mixtures. Atmos. Environ. 34, 3907–3919. http://dx.doi.org/10.1016/S1352-2310(00)00174-6.
Ervens, B., Sorooshian, A., Lim, Y.B., Turpin, B.J., 2014. Key parameters controlling OH-initiated formation of secondary organic aerosol in the aqueous phase (aqSOA). J. Geophys. Res. 119, 3997–4016. http://dx.doi.org/10.1002/2013JD021021.
Fu, X., Guo, H., Wang, X., Ding, X., He, Q., Liu, T., Zhang, Z., 2015. $PM_{2.5}$ acidity at a background site in the Pearl River Delta region in fall-winter of 2007-2012. J. Hazard. Mater 286, 484–492. http://dx.doi.org/10.1016/j.jhazmat.2015.01.022.
Fu, X., Wang, X., Guo, H., Cheung, K., Ding, X., Zhao, X., He, Q., Gao, B., Zhang, Z., Liu, T., Zhang, Y., 2014. Trends of ambient fine particles and major chemical components in the Pearl River Delta region: observation at a regional background site in fall and winter. Sci. Total Environ. 497–498, 274-281. http://dx.doi.org/10.1016/j.scitotenv.2014.08.008.
Gligorovski, S., Strekowski, R., Barbati, S., Vione, D., 2015. Environmental implications of hydroxyl radicals (·OH). Chem. Rev. 115, 13051–13092.
Gordon, T.D., Presto, A.A., Nguyen, N.T., Robertson, W.H., Na, K., Sahay, K.N., Zhang, M., Maddox, C., Rieger, P., Chattopadhyay, S., Maldonado, H., Maricq, M.M., Robinson, A.L., 2014. Secondary organic aerosol production from diesel vehicle exhaust: impact of aftertreatment, fuel chemistry and driving cycle. Atmos. Chem. Phys. 14, 4643–4659. http://dx.doi.org/10.5194/acp-14-4643-2014.
Grosjean, D., Seinfeld, J.H., 1989. Parameterization of the formation potential of secondary organic aerosols. Atmos. Environ. 23 (1967), 1733–1747. http://dx.doi.org/10.1016/0004-6981(89)90058-9.
Hallquist, M., Wenger, J.C., Baltensperger, U., Rudich, Y., Simpson, D., Claeys, M., Dommen, J., Donahue, N.M., George, C., Goldstein, A.H., Hamilton, J.F., Herrmann, H., Hoffmann, T., Iinuma, Y., Jang, M., Jenkin, M.E., Jimenez, J.L., Kiendler-Scharr, A., Maenhaut, W., McFiggans, G., Mentel, T.F., Monod, A., Prevot, A.S.H., Seinfeld, J.H., Surratt, J.D., Szmigielski, R., Wildt, J., 2009. The formation, properties and impact of secondary organic aerosol: current and emerging issues. Atmos. Chem. Phys. 9, 5155–5236. http://dx.doi.org/10.5194/acp-9-5155-2009.
Hildebrandt, L., Donahue, N.M., Pandis, S.N., 2009. High formation of secondary organic aerosol from the photo-oxidation of toluene. Atmos. Chem. Phys. 9, 2973–2986. http://dx.doi.org/10.5194/acp-9-2973-2009.
Hodzic, A., Jimenez, J.L., Madronich, S., Canagaratna, M.R., DeCarlo, P.F., Kleinman, L., Fast, J., 2010. Modeling organic aerosols in a megacity: potential contribution of semi-volatile and intermediate volatility primary organic compounds to secondary organic aerosol formation. Atmos. Chem. Phys. 10, 5491–5514. http://dx.doi.org/10.5194/acp-10-5491-2010.
Hodzic, A., Jimenez, J.L., 2011. Modeling anthropogenically controlled secondary organic aerosols in a megacity: a simplified framework for global and climate models. Geosci. Model Dev. 4, 901–917. http://dx.doi.org/10.5194/gmd-4-901-2011.
Hu, X., Zhang, Y., Ding, Z., Wang, T., Lian, H., Sun, Y., Wu, J., 2012. Bioaccessibility and health risk of arsenic and heavy metals (Cd, Co, Cr, Cu, Ni, Pb, Zn and Mn) in TSP and $PM_{2.5}$ in Nanjing, China. Atmos. Environ. 57, 146–152. http://dx.doi.org/10.1016/j.atmosenv.2012.04.056.
Huang, R.J., Zhang, Y., Bozzetti, C., Ho, K.F., Cao, J.J., Han, Y., Daellenbach, K.R., Slowik, J.G., Platt, S.M., Canonaco, F., Zotter, P., Wolf, R., Pieber, S.M., Bruns, E.A., Crippa, M., Ciarelli, G., Piazzalunga, A., Schwikowski, M., Abbaszade, G., Schnelle-Kreis, J., Zimmermann, R., An, Z., Szidat, S., Baltensperger, U., El Haddad, I., Prevot, A.S., 2014. High secondary aerosol contribution to particulate pollution during haze events in China. Nature 514, 218–222. http://dx.doi.org/10.1038/nature13774.
Hurley, M.D., Sokolov, O., Wallington, T.J., Takekawa, H., Karasawa, M., Klotz, B., Barnes, I., Becker, K.H., 2001. Organic aerosol formation during the atmospheric degradation of toluene. Environ. Sci. Technol. 35, 1358–1366. http://dx.doi.org/10.1021/es0013733.
Jang, M., Czoschke, N.M., Northcross, A.L., Cao, G., Shaof, D., 2006. SOA formation from partitioning and heterogeneous reactions: model study in the presence of inorganic species. Environ. Sci. Technol. 40, 3013–3022. http://dx.doi.org/10.1021/es0511220.
Jayne, J.T., Leard, D.C., Zhang, X., Davidovits, P., Smith, K.A., Kolb, C.E., Worsnop, D.R., 2000. Development of an aerosol mass spectrometer for size and composition analysis of submicron particles. Aerosol Sci. Technol. 33, 49–70. http://dx.doi.org/10.1080/027868200410840.
Jordan, A., Haidacher, S., Hanel, G., Hartungen, E., Märk, L., Seehauser, H., Schottkowsky, R., Sulzer, P., Märk, T.D., 2009. A high resolution and high sensitivity proton-transfer-reaction time-of-flight mass spectrometer (PTR-ToF-MS). Int. J. Mass Spectrom. 286, 122–128. http://dx.doi.org/10.1016/j.ijms.2009.07.005.
Kamens, R.M., Zhang, H., Chen, E.H., Zhou, Y., Parikh, H.M., Wilson, R.L., Galloway, K.E., Rosen, E.P., 2011. Secondary organic aerosol formation from toluene in an atmospheric hydrocarbon mixture: water and particle seed effects. Atmos. Environ. 45, 2324–2334. http://dx.doi.org/10.1016/j.atmosenv.2010.11.007.
Lelieveld, J., Heintzenberg, J., 1992. Sulfate cooling effect on climate through in-cloud oxidation of anthropogenic SO_2. Science 258, 117–120. http://dx.doi.org/10.1126/science.258.5079.117.
Lelieveld, J., Evans, J.S., Fnais, M., Giannadaki, D., Pozzer, A., 2015. The contribution of outdoor air pollution sources to premature mortality on a global scale. Nature 525, 367–371. http://dx.doi.org/10.1038/nature15371.
Li, L.J., Tang, P., Cocker, D.R., 2015. Instantaneous nitric oxide effect on secondary organic aerosol formation from m-xylene photooxidation. Atmos. Environ. 119, 144–155. http://dx.doi.org/10.1016/j.atmosenv.2015.08.010.
Lim, Y.B., Tan, Y., Perri, M.J., Seitzinger, S.P., Turpin, B.J., 2010. Aqueous chemistry and its role in secondary organic aerosol (SOA) formation. Atmos. Chem. Phys. 10, 10521–10539. http://dx.doi.org/10.5194/acp-10-10521-2010.
Lindinger, W., Hansel, A., Jordan, A., 1998. On-line monitoring of volatile organic compounds at pptv levels by means of proton-transfer-reaction mass spectrometry (PTR-MS) medical applications, food control and environmental research. Int. J. Mass Spectrom. Ion. Process. 173, 191–241. http://dx.doi.org/10.1016/S0168-1176(97)00281-4.
Liu, S., Hu, M., Wu, Z., Wehner, B., Wiedensohler, A., Cheng, Y., 2008. Aerosol number size distribution and new particle formation at a rural/coastal site in Pearl River Delta (PRD) of China. Atmos. Environ. 42, 6275–6283. http://dx.doi.org/10.1016/j.atmosenv.2008.01.063.
Liu, T., Wang, X., Deng, W., Hu, Q., Ding, X., Zhang, Y., He, Q., Zhang, Z., Lü, S., Bi, X., Chen, J., Yu, J., 2015a. Secondary organic aerosol formation from photochemical aging of light-duty gasoline vehicle exhausts in a smog chamber. Atmos. Chem. Phys. 15, 9049–9062. http://dx.doi.org/10.5194/acp-15-9049-2015.
Liu, T., Wang, X., Hu, Q., Deng, W., Zhang, Y., Ding, X., Fu, X., Bernard, F., Zhang, Z., Lü, S., He, Q., Bi, X., Chen, J., Sun, Y., Yu, J., Peng, P., Sheng, G., Fu, J., 2016. Formation of secondary aerosols from gasoline vehicle exhaust when mixing with SO_2. Atmos. Chem. Phys. 16, 675–689. http://dx.doi.org/10.5194/acp-16-675-2016.
Liu, Z., Guan, D., Wei, W., Davis, S.J., Ciais, P., Bai, J., Peng, S., Zhang, Q., Hubacek, K., Marland, G., Andres, R.J., Crawford-Brown, D., Lin, J., Zhao, H., Hong, C., Boden, T.A., Feng, K., Peters, G.P., Xi, F., Liu, J., Li, Y., Zhao, Y., Zeng, N., He, K., 2015b. Reduced carbon emission estimates from fossil fuel combustion and cement production in China. Nature 524, 335–338. http://dx.doi.org/10.1038/nature14677.
Mahmud, A., Barsanti, K., 2013. Improving the representation of secondary organic aerosol (SOA) in the MOZART-4 global chemical transport model. Geosci. Model Dev. 6, 961–980. http://dx.doi.org/10.5194/gmd-6-961-2013.
Marais, E.A., Jacob, D.J., Jimenez, J.L., Campuzano-Jost, P., Day, D.A., Hu, W., Krechmer, J., Zhu, L., Kim, P.S., Miller, C.C., Fisher, J.A., Travis, K., Yu, K., Hanisco, T.F., Wolfe, G.M., Arkinson, H.L., Pye, H.O.T., Froyd, K.D., Liao, J., McNeill, V.F., 2016. Aqueous-phase mechanism for secondary organic aerosol formation from isoprene: application to the Southeast United States and co-benefit of SO_2 emission controls. Atmos. Chem. Phys. 16, 1603–1618. http://dx.doi.org/10.5194/acp-16-1603-2016.
Ng, N.L., Kroll, J.H., Chan, A.W.H., Chhabra, P.S., Flagan, R.C., Seinfeld, J.H., 2007. Secondary organic aerosol formation from m-xylene, toluene, and benzene. Atmos. Chem. Phys. 7, 3909–3922. http://dx.doi.org/10.5194/acp-7-3909-2007.
Nishino, N., Arey, J., Atkinson, R., 2010. Formation yields of glyoxal and methylglyoxal from the gas-phase OH radical-initiated reactions of toluene, xylenes, and trimethylbenzenes as a function of NO_2 concentration. J. Phys. Chem. A 114, 10140–10147. http://dx.doi.org/10.1021/jp105112h.
Nordin, E.Z., Eriksson, A.C., Roldin, P., Nilsson, P.T., Carlsson, J.E., Kajos, M.K., Hellén, H., Wittbom, C., Rissler, J., Löndahl, J., Swietlicki, E., Svenningsson, B., Bohgard, M., Kulmala, M., Hallquist, M., Pagels, J.H., 2013. Secondary organic aerosol formation from idling gasoline passenger vehicle emissions investigated in a smog chamber. Atmos. Chem. Phys. 13, 6101–6116. http://dx.doi.org/10.5194/acp-13-6101-2013.
Odum, J.R., Hoffmann, T., Bowman, F., Collins, D., Flagan, R.C., Seinfeld, J.H., 1996. Gas/particle partitioning and secondary organic aerosol yields. Environ. Sci. Technol. 30, 2580–2585. http://dx.doi.org/10.1021/es950943+.
Odum, J.R., Jungkamp, T.P.W., Griffin, R.J., Flagan, R.C., Seinfeld, J.H., 1997a. The atmospheric aerosol-forming potential of whole gasoline vapor. Science 276, 96–99. http://dx.doi.org/10.1126/science.276.5309.96.
Odum, J.R., Jungkamp, T.P.W., Griffin, R.J., Forstner, H.J.L., Flagan, R.C., Seinfeld, J.H., 1997b. Aromatics, reformulated gasoline, and atmospheric organic aerosol formation. Environ. Sci. Technol. 31, 1890–1897. http://dx.doi.org/10.1021/es960535l.
Parrish, D.D., Zhu, T., 2009. Clean air for megacities. Science 326, 674–675. http://dx.doi.org/10.1126/science.1176064.
Pope, C.A., Ezzati, M., Dockery, D.W., 2009. Fine-particulate air pollution and life expectancy in the United States. N. Engl. J. Med. 360, 376–386. http://dx.doi.org/10.1056/NEJMsa0805646.
Pye, H.O., Pinder, R.W., Piletic, I.R., Xie, Y., Capps, S.L., Lin, Y.H., Surratt, J.D., Zhang, Z., Gold, A., Luecken, D.J., Hutzell, W.T., Jaoui, M., Offenberg, J.H., Kleindienst, T.E., Lewandowski, M., Edney, E.O., 2013. Epoxide pathways improve model predictions of isoprene markers and reveal key role of acidity in aerosol formation.

Environ. Sci. Technol. 47, 11056–11064. http://dx.doi.org/10.1021/es402106h.
Robinson, A.L., Donahue, N.M., Shrivastava, M.K., Weitkamp, E.A., Sage, A.M., Grieshop, A.P., Lane, T.E., Pierce, J.R., Pandis, S.N., 2007. Rethinking organic aerosols: semivolatile emissions and photochemical aging. Science 315, 1259–1262. http://dx.doi.org/10.1126/science.1133061.
Song, C., Na, K., Cocker, D.R., 2005. Impact of the hydrocarbon to NO_x ratio on secondary organic aerosol formation. Environ. Sci. Technol. 39, 3143–3149. http://dx.doi.org/10.1021/es0493244.
Surratt, J.D., Michael, Lewandowski, Offenberg John, H., Mohammed, Jaoui, Kleindienst Tadeusz, E., Edney Edward, O., Seinfeld John, H., 2007. Effect of acidity on secondary organic aerosol formation from isoprene. Environ. Sci. Technol. 41, 5363–5369. http://dx.doi.org/10.1021/es0704176.
Tsimpidi, A.P., Karydis, V.A., Zavala, M., Lei, W., Molina, L., Ulbrich, I.M., Jimenez, J.L., Pandis, S.N., 2010. Evaluation of the volatility basis-set approach for the simulation of organic aerosol formation in the Mexico City metropolitan area. Atmos. Chem. Phys. 10, 525–546. http://dx.doi.org/10.5194/acp-10-525-2010.
Volkamer, R., Jimenez, J.L., San Martini, F., Dzepina, K., Zhang, Q., Salcedo, D., Molina, L.T., Worsnop, D.R., Molina, M.J., 2006. Secondary organic aerosol formation from anthropogenic air pollution: rapid and higher than expected. Geophys. Res. Lett. 33, L17811. http://dx.doi.org/10.1029/2006GL026899.
Wang, S., Wu, D., Wang, X.-M., Fung, J.C.-H., Yu, J.Z., 2013. Relative contributions of secondary organic aerosol formation from toluene, xylenes, isoprene, and monoterpenes in Hong Kong and Guangzhou in the Pearl River Delta, China: an emission-based box modeling study. J. Geophys. Res. 118, 507–519. http://dx.doi.org/10.1029/2012JD017985.
Wang, X., Ding, X., Fu, X., He, Q., Wang, S., Bernard, F., Zhao, X., Wu, D., 2012. Aerosol scattering coefficients and major chemical compositions of fine particles observed at a rural site in the central Pearl River Delta, South China. J. Environ. Sci. 24, 72–77. http://dx.doi.org/10.1016/S1001-0742(11)60730-4.
Wang, X., Liu, T., Bernard, F., Ding, X., Wen, S., Zhang, Y., Zhang, Z., He, Q., Lu, S., Chen, J., Saunders, S., Yu, J., 2014. Design and characterization of a smog chamber for studying gas-phase chemical mechanisms and aerosol formation. Atmos. Meas. Tech. 7, 301–313. http://dx.doi.org/10.5194/amt-7-301-2014.
Wang, X., Wu, T., 2008. Release of isoprene and monoterpenes during the aerobic decomposition of orange wastes from laboratory incubation experiments. Environ. Sci. Technol. 42, 3265–3270. http://dx.doi.org/10.1021/es702999j.
Weitkamp, E.A., Sage, A.M., Pierce, J.R., Donahue, N.M., Robinson, A.L., 2007. Organic aerosol formation from photochemical oxidation of diesel exhaust in a smog chamber. Environ. Sci. Technol. 41, 6969–6975. http://dx.doi.org/10.1021/es070193r.
Wexler, A.S., Clegg, S.L., 2002. Atmospheric aerosol models for systems including the ions H^+, NH_4^+, Na^+, SO_4^{2-}, NO_3^-, Cl^-, Br^-, and H_2O. J. Geophys. Res. 107 (D14), 4207. http://dx.doi.org/10.1029/2001JD000451.
Xu, L., Guo, H., Boyd, C.M., Klein, M., Bougiatioti, A., Cerully, K.M., Hite, J.R., Isaacman-VanWertz, G., Kreisberg, N.M., Knote, C., Olson, K., Koss, A., Goldstein, A.H., Hering, S.V., de Gouw, J., Baumann, K., Lee, S.-H., Nenes, A., Weber, R.J., Ng, N.L., 2015. Effects of anthropogenic emissions on aerosol formation from isoprene and monoterpenes in the Southeastern United States. Proc. Natl. Acad. Sci. U. S. A. 112, 37–42. http://dx.doi.org/10.1073/pnas.1512279112.
Yang, W., He, H., Ma, Q., Ma, J., Liu, Y., Liu, P., Mu, Y., 2016. Synergistic formation of sulfate and ammonium resulting from reaction between SO_2 and NH_3 on typical mineral dust. Phys. Chem. Chem. Phys. 18, 956–964. http://dx.doi.org/10.1039/C5CP06144J.
Ye, J., Gordon, C.A., Chan, A.W.H., 2016a. Enhancement in secondary organic aerosol formation in the presence of preexisting organic particle. Environ. Sci. Technol. 50, 3572–3579. http://dx.doi.org/10.1021/acs.est.5b05512.
Ye, P.L., Ding, X., Hakala, J., Hofbauer, V., Robinson, E.S., Donahue, N.M., 2016b. Vapor wall loss of semi-volatile organic compounds in a Teflon chamber. Aerosol Sci. Technol. 50, 822–834. http://dx.doi.org/10.1080/02786826.2016.1195905.
Yeh, G.K., Ziemann, P.J., 2014. Alkyl nitrate formation from the Reactions of C_8–C_{14} n-Alkanes with OH radicals in the presence of NO_x: measured yields with essential corrections for gas–wall partitioning. J. Phys. Chem. A 118, 8147–8157. http://dx.doi.org/10.1021/jp500631v.
Yue, D.L., Hu, M., Wu, Z.J., Guo, S., Wen, M.T., Nowak, A., Wehner, B., Wiedensohler, A., Takegawa, N., Kondo, Y., Wang, X.S., Li, Y.P., Zeng, L.M., Zhang, Y.H., 2010. Variation of particle number size distributions and chemical compositions at the urban and downwind regional sites in the Pearl River Delta during summertime pollution episodes. Atmos. Chem. Phys. 10, 9431–9439. http://dx.doi.org/10.5194/acp-10-9431-2010.
Zhang, Q., Jimenez, J.L., Canagaratna, M.R., Allan, J.D., Coe, H., Ulbrich, I., Alfarra, M.R., Takami, A., Middlebrook, A.M., Sun, Y.L., Dzepina, K., Dunlea, E., Docherty, K., DeCarlo, P.F., Salcedo, D., Onasch, T., Jayne, J.T., Miyoshi, T., Shimono, A., Hatakeyama, S., Takegawa, N., Kondo, Y., Schneider, J., Drewnick, F., Borrmann, S., Weimer, S., Demerjian, K., Williams, P., Bower, K., Bahreini, R., Cottrell, L., Griffin, R.J., Rautiainen, J., Sun, J.Y., Zhang, Y.M., Worsnop, D.R., 2007. Ubiquity and dominance of oxygenated species in organic aerosols in anthropogenically-influenced Northern Hemisphere midlatitudes. Geophys. Res. Lett. 34. http://dx.doi.org/10.1029/2007gl029979.
Zhang, X., Cappa, C.D., Jathar, S.H., McVay, R.C., Ensberg, J.J., Kleeman, M.J., Seinfeld, J.H., 2014. Influence of vapor wall loss in laboratory chambers on yields of secondary organic aerosol. Proc. Natl. Acad. Sci. U. S. A. 111, 5802–5807. http://dx.doi.org/10.1073/pnas.1404727111.
Zhang, X., Schwantes, R.H., McVay, R.C., Lignell, H., Coggon, M.M., Flagan, R.C., Seinfeld, J.H., 2015. Vapor wall deposition in Teflon chambers. Atmos. Chem. Phys. 15, 4197–4214, 4197-4214. http://dx.doi.org/10.5194/acp-15-4197-2015.
Zhang, Y., Wang, X., Barletta, B., Simpson, I.J., Blake, D.R., Fu, X., Zhang, Z., He, Q., Liu, T., Zhao, X., Ding, X., 2013a. Source attributions of hazardous aromatic hydrocarbons in urban, suburban and rural areas in the Pearl River Delta (PRD) region. J. Hazard. Mater 250–251, 403-411. http://dx.doi.org/10.1016/j.jhazmat.2013.02.023.
Zhang, Y., Wang, X., Blake, D.R., Li, L., Zhang, Z., Wang, S., Guo, H., Lee, F.S.C., Gao, B., Chan, L., Wu, D., Rowland, F.S., 2012. Aromatic hydrocarbons as ozone precursors before and after outbreak of the 2008 financial crisis in the Pearl River Delta region, South China. J. Geophys. Res. 117, D15306. http://dx.doi.org/10.1029/2011JD017356.
Zhang, Y., Wang, X., Zhang, Z., Lü, S., Shao, M., Lee, F.S.C., Yu, J., 2013b. Species profiles and normalized reactivity of volatile organic compounds from gasoline evaporation in China. Atmos. Environ. 79, 110–118. http://dx.doi.org/10.1016/j.atmosenv.2013.06.029.
Zhang, Y.L., Guo, H., Wang, X.M., Simpson, I.J., Barletta, B., Blake, D.R., Meinardi, S., Rowland, F.S., Cheng, H.R., Saunders, S.M., Lam, S.H.M., 2010. Emission patterns and spatiotemporal variations of halocarbons in the Pearl River Delta region, Southern China. J. Geophys. Res. 115, D15309. http://dx.doi.org/10.1029/2009JD013726.
Zhang, Z., Zhang, Y., Wang, X., Lü, S., Huang, Z., Huang, X., Yang, W., Wang, Y., Zhang, Q., 2016. Spatiotemporal patterns and source implications of aromatic hydrocarbons at six rural sites across China's developed coastal regions. J. Geophys. Res. 121, 6669–6687. http://dx.doi.org/10.1002/2016JD025115.
Zhao, L., Wang, X., He, Q., Wang, H., Sheng, G., Chan, L.Y., Fu, J., Blake, D.R., 2004. Exposure to hazardous volatile organic compounds, PM_{10} and CO while walking along streets in urban Guangzhou, China. Atmos. Environ. 38, 6177–6184. http://dx.doi.org/10.1016/j.atmosenv.2004.07.025.